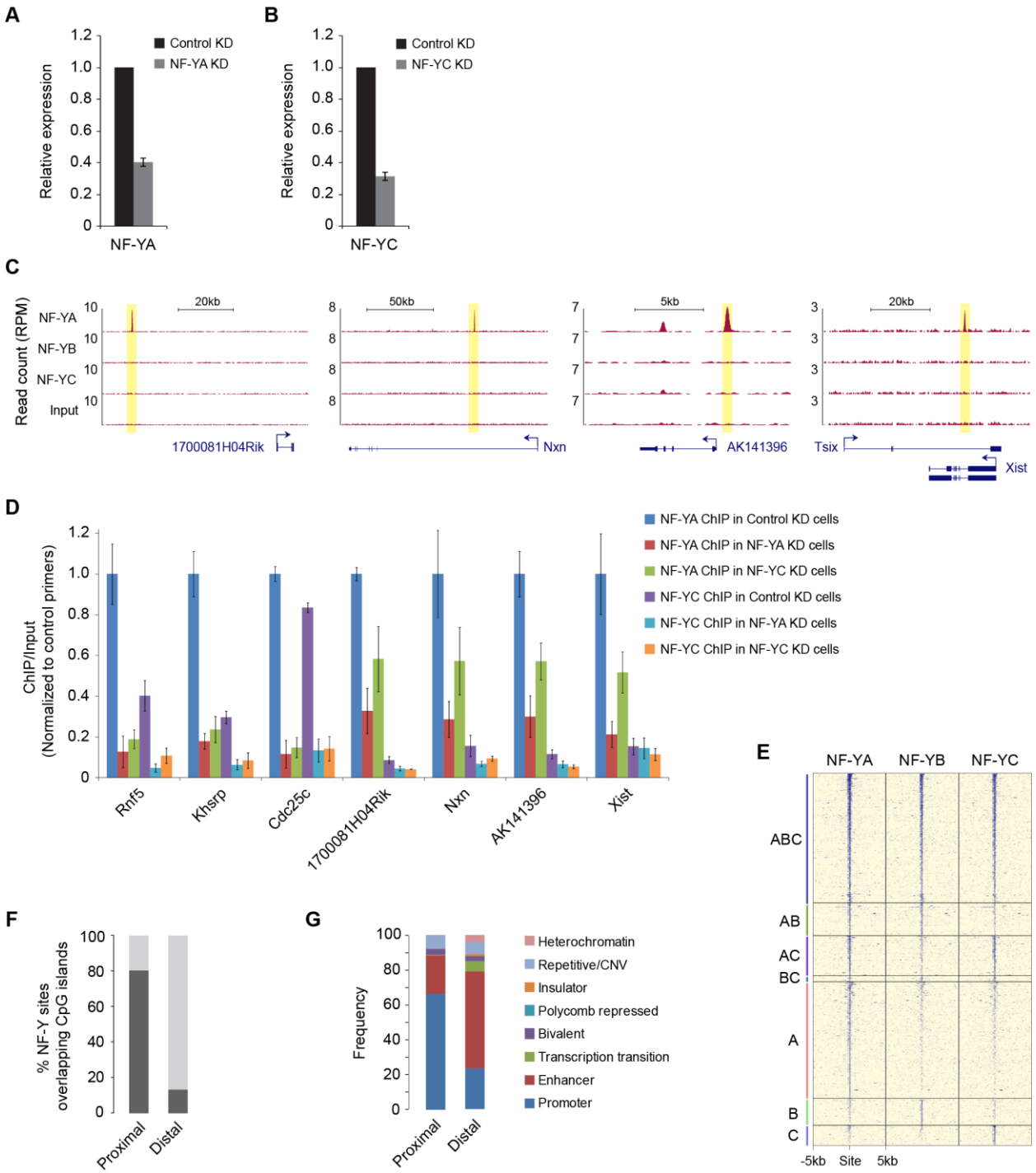

Figure S1 (related to Figure 1). NF-Y binding requires all three subunits

(A-B) RT-qPCR analysis showing relative mRNA levels of *NF-YA* and *NF-YC* in *NF-YA* KD (A) and *NF-YC* KD (B) ESCs (48h), respectively. Data are normalized to *Actin*, *HAZ*, and *TBP*. Error bars represent S.E.M. of three experiments.

(C) Genome browser shots showing NF-YA occupancy at the promoters of *1700081H04Rik*, *Nxn*, *AK141396*, and *Xist* genes, but not NF-YB and NF-YC, the other two subunits of the NF-Y complex.

(D) ChIP-qPCR analysis of the NF-YA and NF-YC occupancy in Control KD, *NF-YA* KD, and *NF-YC* KD ESCs 48h after siRNA transfection. Error bars represent S.E.M. of three experiments.

(E) Heatmap representation of NF-YA, NF-YB, and NF-YC occupancy (ChIP-Seq read density) near called sites bound by NF-YA, NF-YB, NF-YC, or a combination of the three.

(F) Percent of NF-Y sites overlapping CpG islands. Proximal, NF-Y sites within 500 bp of TSSs; Distal, NF-Y sites that are >500 bp away from TSSs.

(G) Annotation of proximal and distal NF-Y sites using chromatin state maps (Ernst and Kellis, 2012).

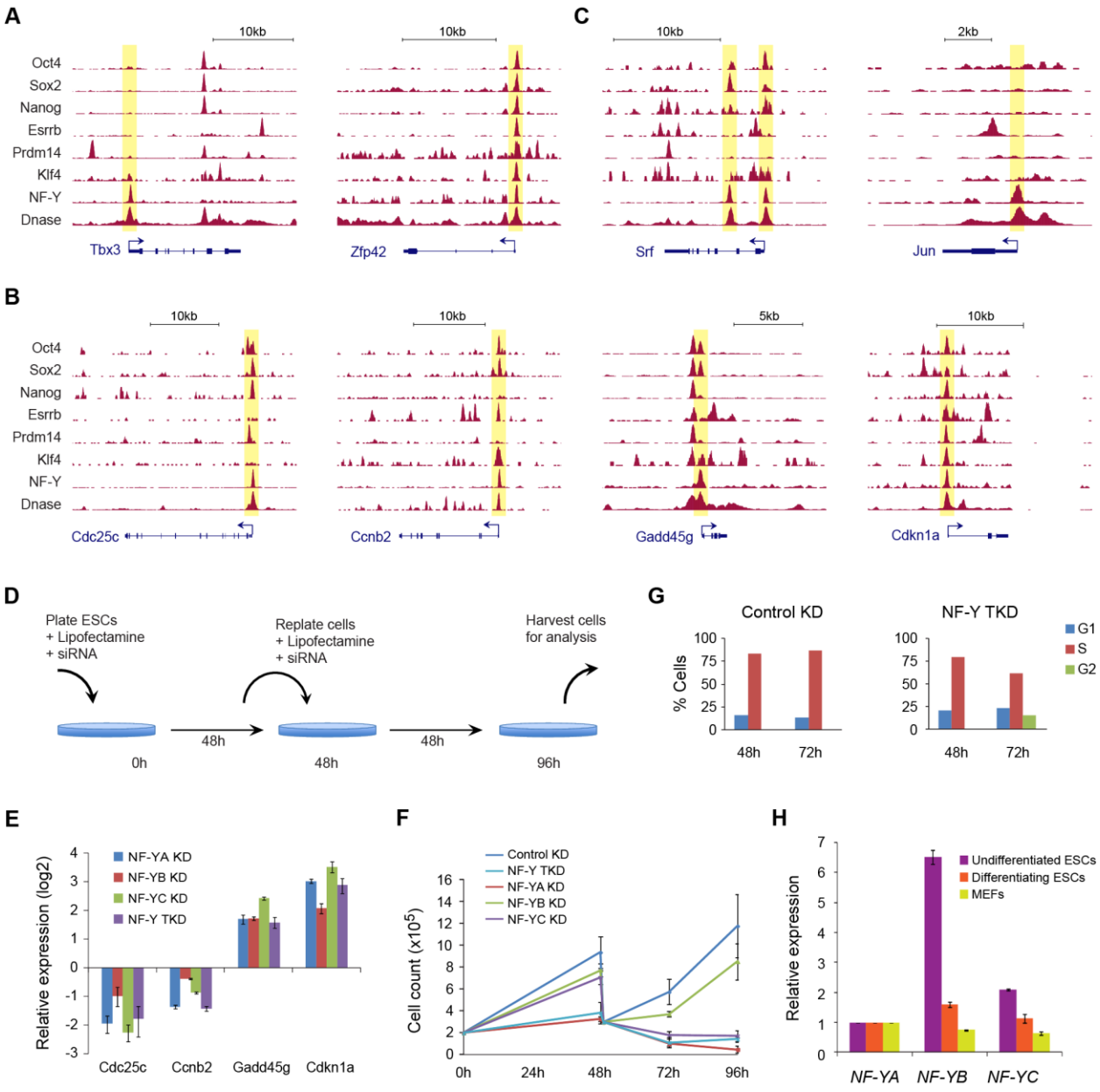

Figure S2 (related to Figure 3). NF-Y controls ESC proliferation by regulating the expression of key cell cycle genes

(A) Genome browser shots showing TF occupancy at pluripotency-associated genes *Tbx3* and *Zfp42*.

(B) Genome browser shots showing TF occupancy at cell cycle genes *Cdc25c*, *Ccnb2*, *Gadd45g*, and *Cdkn1a* (*p21*).

(C) Genome browser shots showing TF occupancy at differentiation genes *Srf* and *Jun*.

(D) Schematic showing siRNA transfection strategy.

(E) RT-qPCR analysis of relative mRNA levels of cell cycle genes shown in (B) in *NF-YA* KD, *NF-YB* KD, *NF-YC* KD, and NF-Y TKD ESCs compared to control KD ESCs 96h after siRNA transfection. Data are normalized to *Actin*, *HAZ*, and *TBP*. Error bars represent S.E.M. of three experiments.

(F) Cell proliferation growth curves were determined by counting the cell numbers in control KD, *NF-YA* KD, *NF-YB* KD, *NF-YC* KD, and NF-Y TKD ESCs at 48h, 72h, and 96h after siRNA transfection. Cells were replated and retransfected at 48h after the initial transfection. The average cell numbers from three experiments are shown. Error bars represent with S.E.M. of three experiments.

(G) Cell cycle distribution measured by flow cytometry analysis in control KD and NF-Y TKD ESCs 48h and 72h after siRNA transfection.

(H) RT-qPCR analysis of relative mRNA levels of NF-Y subunits *NF-YA*, *NF-YB*, and *NF-YC* in wild-type mouse ESCs. Error bars represent S.E.M. of three experiments.

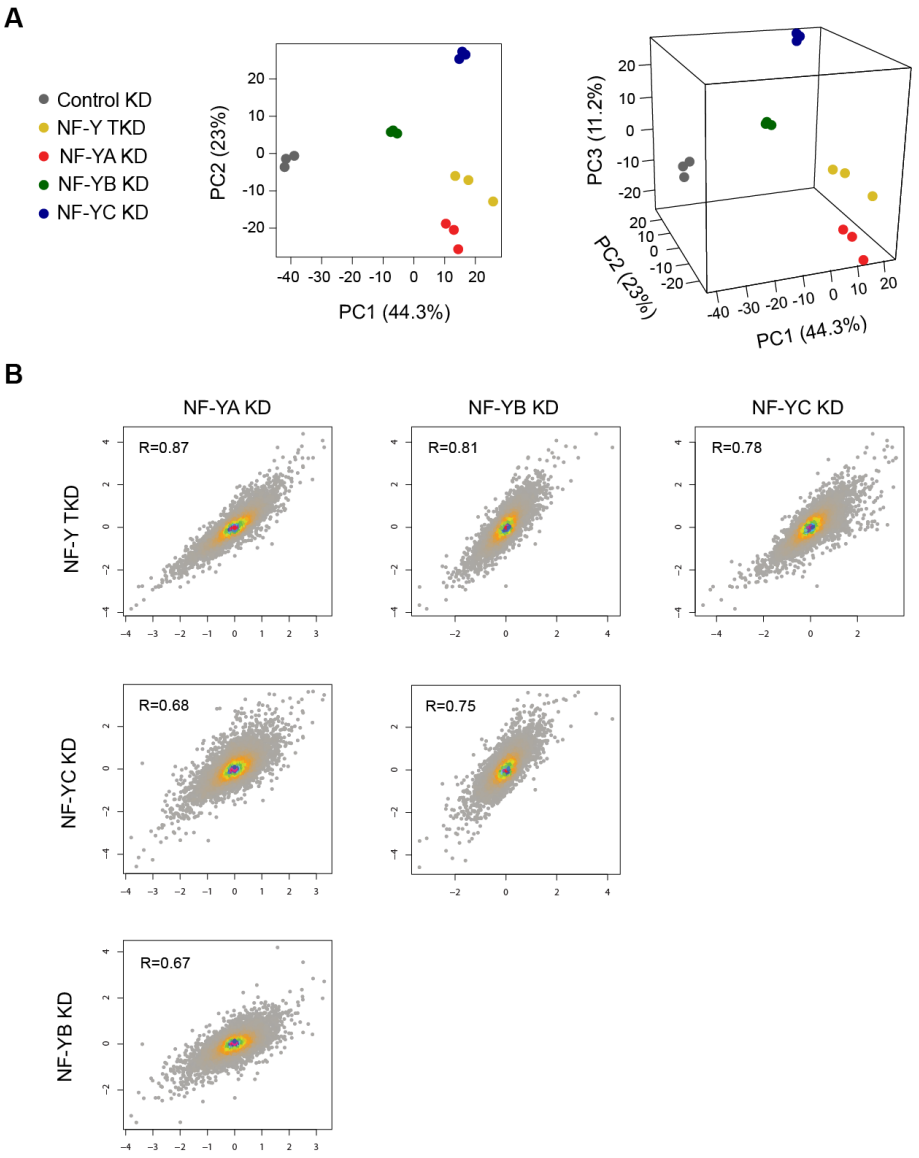

Figure S3 (related to Figure 4). Global gene expression changes upon depletion of individual or all NF-Y subunits are correlated.

(A) Principal component analysis (PCA) of gene expression profiles showing Control KD, *NF-YA* KD, *NF-YB* KD, *NF-YC* KD, and NF-Y TKD ESCs. Each dot represents a biological replicate.

(B) Scatter plots showing pair-wise correlation of global gene expression changes upon *NF-YA* KD, *NF-YB* KD, *NF-YC* KD, and NF-Y TKD ESCs compared to control KD ESCs.

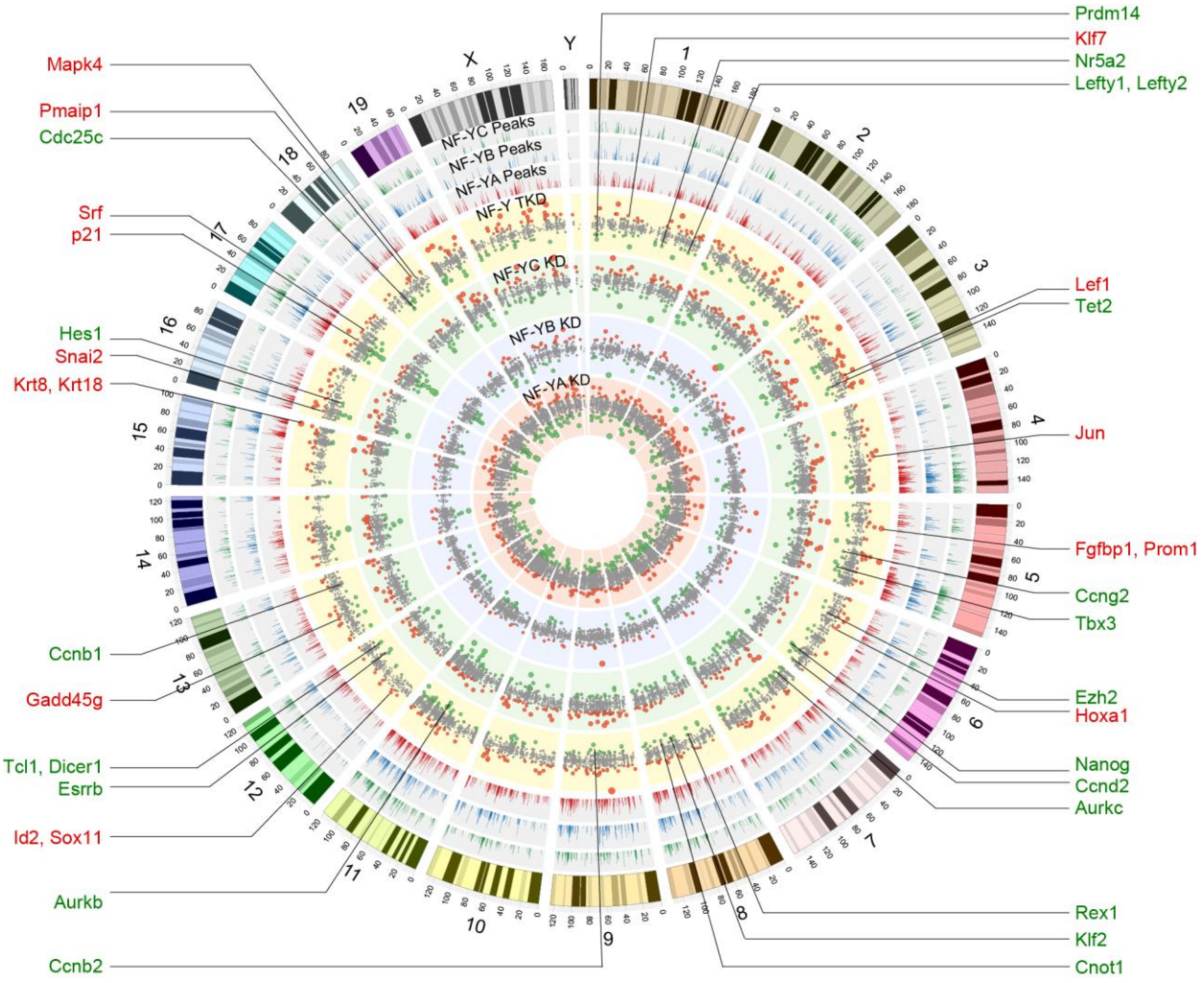

Figure S4 (related to Figure 4). NF-Y regulates key ESC identity and cell cycle genes. Circos plot depicting NF-YA, NF-YB, and NF-YC binding sites across the genome (outer-most tracks). Y-axis represents the peak height for binding sites. Also shown are gene expression fold changes upon *NF-YA* KD, *NF-YB* KD, *NF-YC* KD, and NF-Y TKD (inner-most tracks). Genes whose expression increases (or decreases) by two or more fold are denoted by red (green, respectively) circles, with the size of the circle denoting the magnitude of the change. Selected genes that bind NF-Y and whose expression ≥2-fold are highlighted.

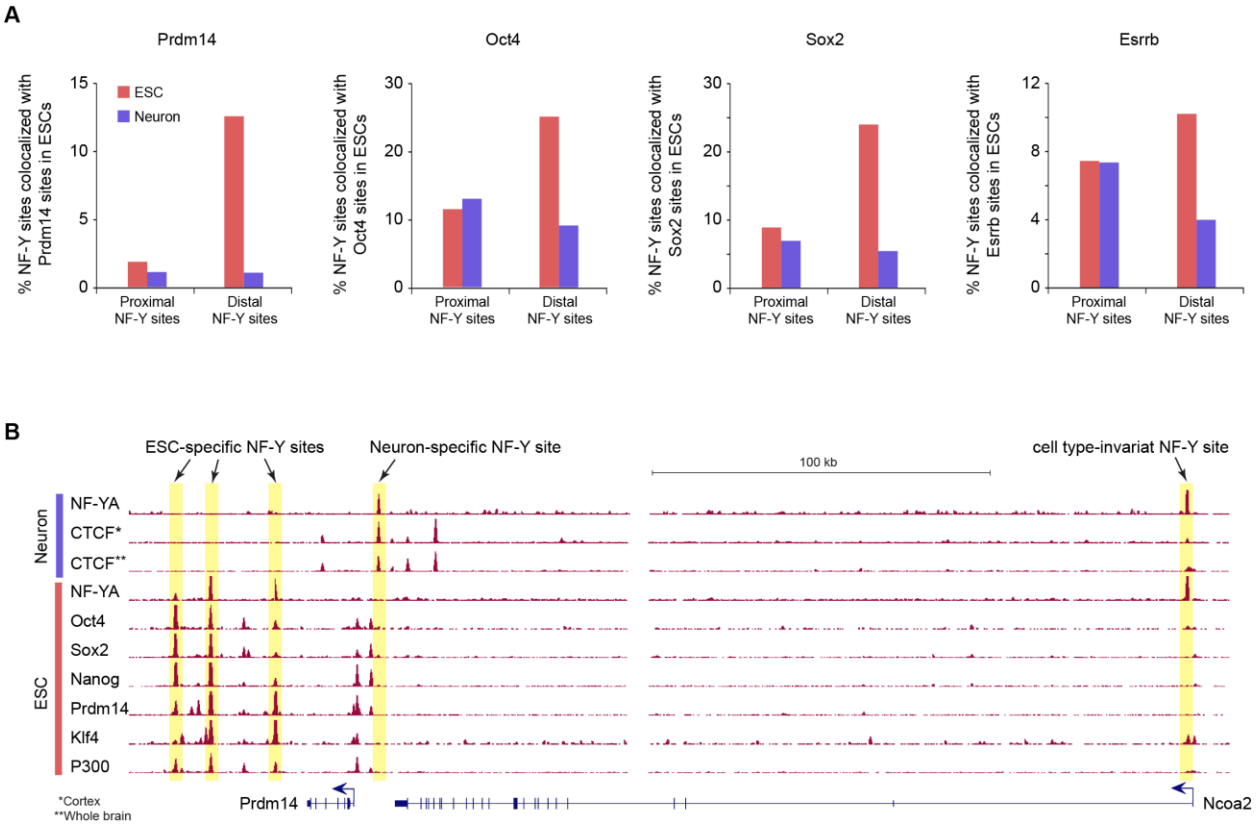

Figure S5 (related to Figure 5). TF co-occupancy at proximal and ESC-specific and neuron-specific distal NF-Y sites.

(A) Master ESC TF co-occupancy at proximal and ESC-specific (red) and neuron-specific (purple) distal NF-Y sites in ESCs

(B) Genome browser shot showing TF occupancy in ESCs and neurons at *Prdm14-Ncoa2* locus. ESC-specific, neuron-specific, and cell type-invariant NF-Y sites are highlighted.

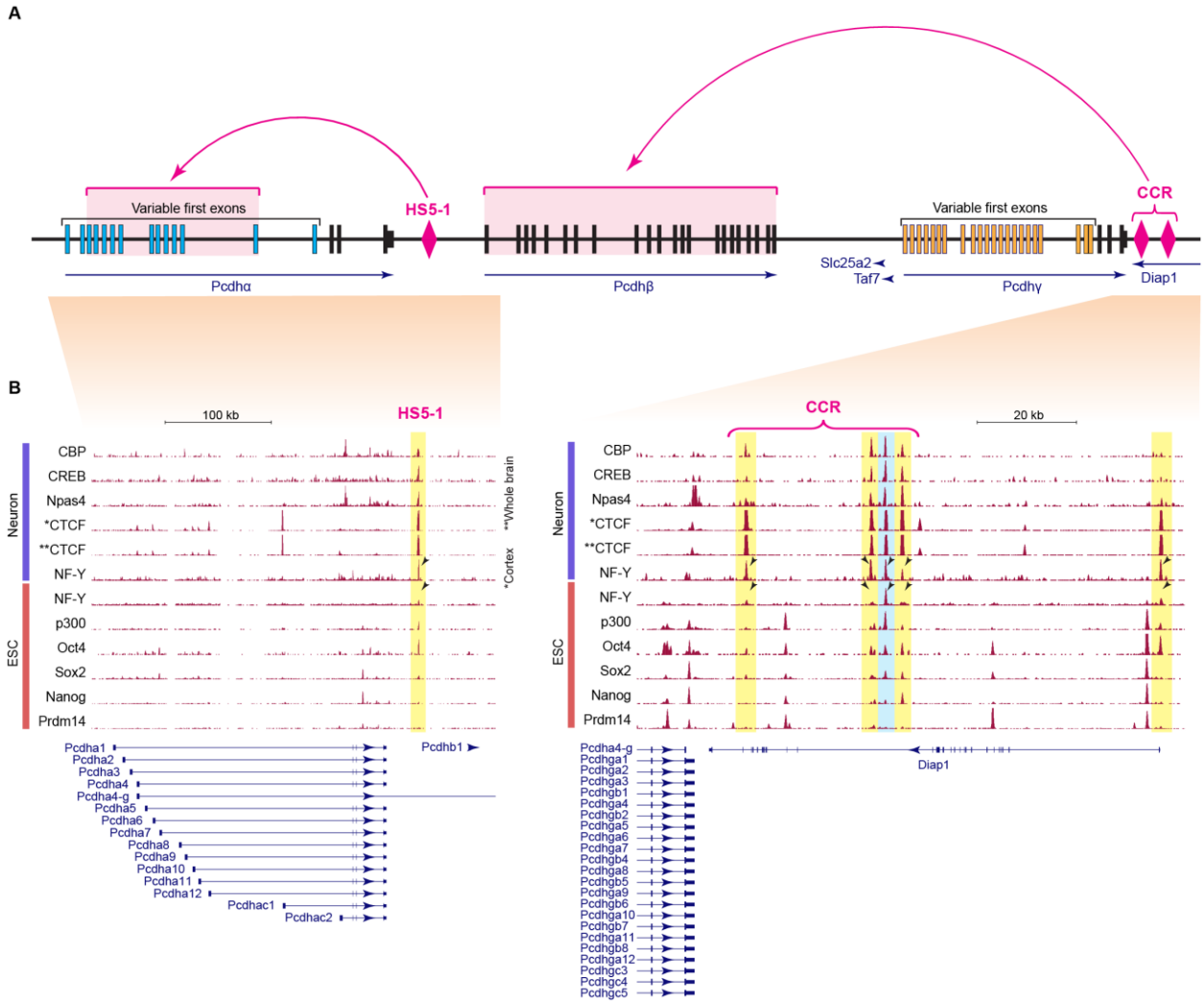

Figure S6 (related to Figure 5). NF-Y colocalizes, in a neuronal specific manner, with CTCF at sites controlling clustered Protocadherin expression.

(A) Genomic structure of the clustered Pcdh gene locus, adapted from Hirayama et al (Hirayama et al., 2012). Rectangles represent exons. Pink diamonds represent enhancer regions (HS5-1 enhances Pcdhα3–α12 and Pcdhαc1; CCR enhances Pcdhaβ1–β22).

(B) Genome browser shot showing TF occupancy in ESCs and neurons at the *Pcdh* gene locus. Neuron-specific and cell type-invariant NF-Y sites are highlighted in yellow and blue, respectively.

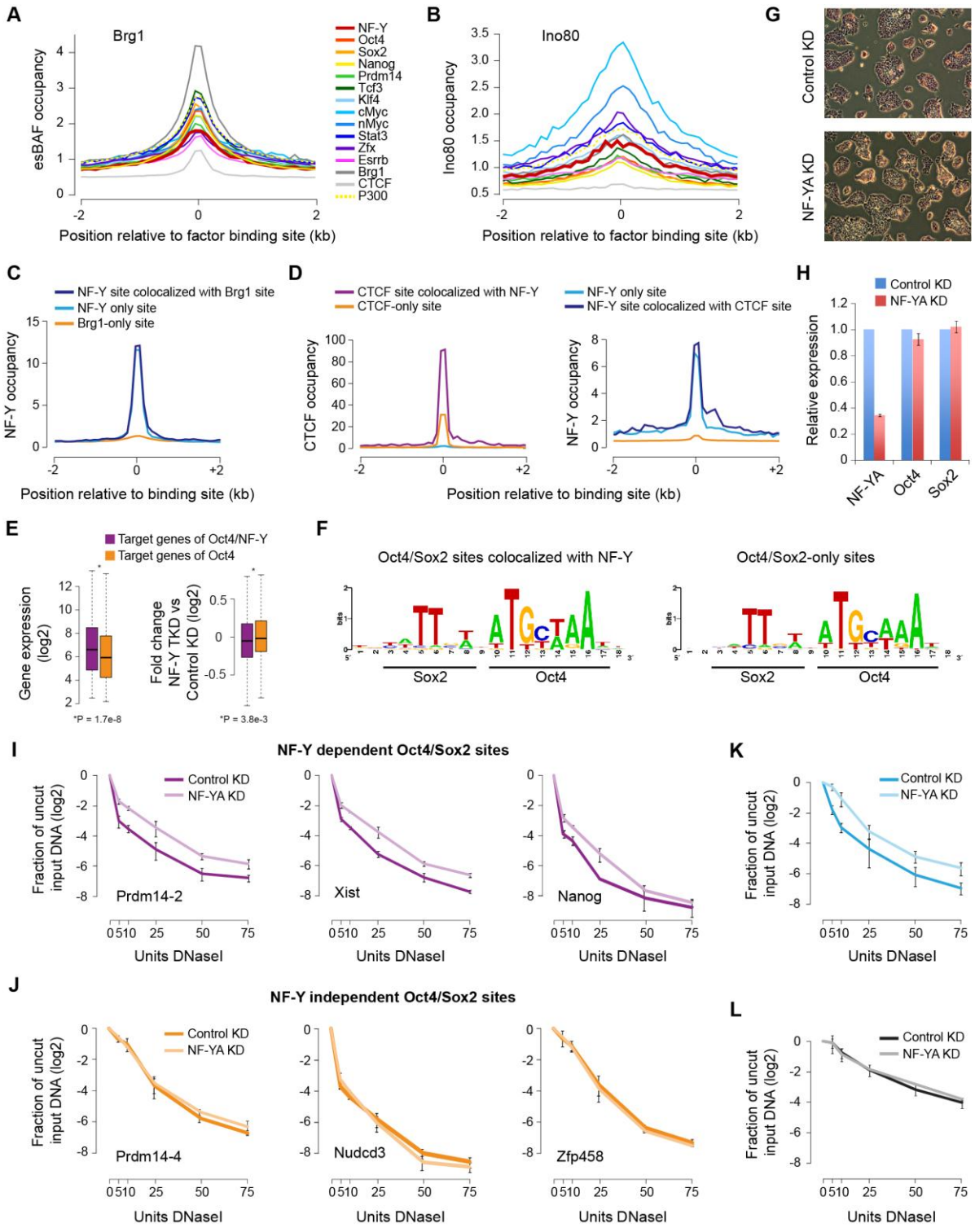

Figure S7 (related to Figures 6 and 7). Depletion of NF-Y diminishes chromatin accessibility at sites co-bound by NF-Y and Oct4/Sox2 but not at sites bound only by Oct4/Sox2.

(A) Chromatin remodeling complex esBAF occupancy, as measured by Brg1 ChIP-Seq (Ho et al., 2009) at various TF (distal) binding sites in ESCs.

(B) Chromatin remodeling complex Ino80 occupancy, as measured by Ino80 ChIP-Seq (Wang et al., 2014), at various TF (distal) binding sites in ESCs. Colors and labels same as in Figure S7A.
(C) NF-Y occupancy at distal NF-Y sites colocalized with Brg1 (blue), distal NF-Y-only sites (cyan), and distal Brg1 only sites (orange).
(D) CTCF (left) and NF-Y (right) occupancy at distal CTCF sites colocalized with NF-Y (purple), distal CTCF-only sites (orange), distal NF-Y sites colocalized with CTCF (cyan), and distal NF-Y only sites (blue).
(E) *Left*: Expression levels of target genes of Oct4 with and without NF-Y co-occupancy in control ESCs. *Right*: Expression fold change of target genes of Oct4 with and without NF-Y co-occupancy in NF-Y TKD vs Control KD ESCs.
(F) Consensus sequence motif enriched within Oct4/Sox2 binding sites with and without NF-Y co-occupancy using *de novo* motif analysis.
(G) Morphology and alkaline phosphatase staining of control KD and *NF-YA* KD ESCs 48h after siRNA transfection.
(H) RT-qPCR analysis of relative mRNA levels of NF-Y subunits *NF-YA*, *Oct4*, and *Sox2* in Control and NF-YA KD ESCs. Data are normalized to *Actin*, *HAZ*, and *TBP*. Error bars represent S.E.M. of three experiments.
(I) DNase I and qPCR analysis of NF-Y dependent Oct4/Sox2 sites (n = 3 each) in Control and NF-YA KD ESCs. Error bars represent S.E.M. of four experiments.
(J) DNase I and qPCR analysis of NF-Y independent Oct4/Sox2 sites (n = 3 each) in Control and NF-YA KD ESCs. Error bars represent S.E.M. of four experiments.
(K) DNase I and qPCR analysis of a distal NF-Y site within the Srf gene, bound by NF-Y (but not Oct4, Sox2, Nanog, Prdm14, Esrrb or Klf4), in Control and NF-YA KD ESCs. Error bars represent S.E.M. of four experiments.
(L) DNase I and qPCR analysis of a control site, that does not bind NF-Y, in Control and NF-YA KD ESCs. Error bars represent S.E.M. of four experiments.

Table S1 (related to Figures 1, 5, 6, and 7). Primers used for ChIP-qPCR and DNase I hypersensitivity analysis

Primer name	Forward primer	Reverse primer
1700081H04Rik	AGGGTCCGGTAACTCCTCTC	GGCTCATACCTGTCGTTCCA
AK141396	CAGCACACAGGAGGAGGACT	CGGCTGGTCTCTAACTGCAT
Calm2	AGGGCCATTCACAACAAAAG	TGTTAGGATGCGTGCTTGTC
Cdc25c	GGAACAGAAGCGATTCTTCG	TCATGTTCTGGTGCGATGAT
Esrrb	TGGGAAGTGTTGCTATTCCA	TCAGAGCTCCAGATCCCCTA
Foxi3	GGCCTCGAGGTTAGAGTCCT	AGGGAACTAGCGTGTTCAGC
Khsrp	CGGCAAGATAGTCGTCAACA	AGTCACGTCCAAATCCAAGC
Nanog	CCGCTCCTTTTCAGCACTAA	CAGGGAAGCGGTTTGAATAG
NR_040693	AGGGTCCGGTAACTCCTCTC	GGCTCATACCTGTCGTTCCA
Nudcd3	GGATGTGTGCAATGTTGAGG	CTCACTTCCGCTCCTTCTGT
Nxn	CAACTGTCGACTGTGCGTTT	TAGCTTTGACTGCCCTGACC
Paip2b	GAGAATGCCGCTCACTTACC	TCAGAGCTGGGAGTCTCCAT
Prdm14-2	AAGCAGCAGGGTGGAGATAA	CAAACGGATTGGAGGTTGAT
Prdm14-4	GCAAATTAGGCTCATTCGTG	AATCCTCGGGAGTTCTGGTT
Rnf5	ACCCTTGCACGATGATGATT	CGAGTTCTGTAGGCCTGAGC
Srf	AGGCCTTGAGAACCAAGCTA	AACGCCTTTACCAATCAACG
Xist1	AACCCTTTTAAGTCCACTGTAAATTCC	TAGAGAGCCAGACAATGCTAAGCC
Zfp568	TCCGCCCCTATATCTTGTTG	CTGGGTCTCTGGACTTCAGG
Zic3	CCGCAGCTACCCAATCAG	AATCACTCACTCCTCGCACA
Ager (control #1)	ACCCCACTCAGACATGAACC	TGGCAATTCCCCTCAGTTAG
chr8 (control #2)	AAGGGGCCTCTGCTTAAAAA	AGAGCTCCATGGCAGGTAGA
Pdp2 (control #3)	CTGGACCTCTCTGGTTCTGG	TTGGCCTCTTAGCGACAAGT
Tmem179 (control #4)	TTCCGTGTCCCCAGAATAAG	TTAAGCCATCCACTCCCTTG
Tpg (control #5)	TGGAGCTCTTTCATGTTCTTCCTT	ATGAATGGGCTTCTTGAATTTCTACT

Table S2 (related to Figures 3 and 4). Gene specific primers used for RT-qPCR analysis

Primer name	**Forward primer**	**Reverse primer**
Brachyury	ACCCAGACTCGCCCAATTT	CACGATGTGAATCCGAGGTT
Ccnb2	ACTGGCTGGTCCAAGTCCAT	ATATTTGGAAGCCAGGAGCA
Cdc25c	TTCAGAAGACCCAATGGAGTG	GAATGGCGTTCATGTCACAG
Cdkn1a	TTGCCAGCAGAATAAAAGGTG	TTTGCTCCTGTGCGGAAC
Cdx2	AGGCTGAGCCATGAGGAGTA	CGAGGTCCATAATTCCACTCA
Eomes	ACCGGCACCAAACTGAGA	AAGCTCAAGAAAGGAAACATGC
Esrrb	CAGGCAAGGATGACAGACG	GAGACAGCACGAAGGACTGC
Fgf5	AAAACCTGGTGCACCCTAGA	CATCACATTCCCGAATTAAGC
Foxa2	CGAGCTAAAGGGAGCACCT	TAATGGTGCTCGGGCTTC
Gadd45g	GGATAACTTGCTGTTCGTGGA	AAGTTCGTGCAGTGCTTTCC
Gata3	TTATCAAGCCCAAGCGAAG	TGGTGGTGGTCTGACAGTTC
Gata4	GGAAGACACCCCAATCTCG	CATGGCCCCACAATTGAC
Gata6	GGTCTCTACAGCAAGATGAATGG	TGGCACAGGACAGTCCAAG
Hand1	CAAGCGGAAAAGGGAGTTG	GTGCGCCCTTTAATCCTCTT
Id2	GACAGAACCAGGCGTCCA	AGCTCAGAAGGGAATTCAGATG
Krt18	AGATGACACCAACATCACAAGG	TCCAGACCTTGGACTTCCTC
Krt8	AGTTCGCCTCCTTCATTGAC	GCTGCAACAGGCTCCACT
Lefty1	ACTCAGTATGTGGCCCTGCTA	AACCTGCCTGCCACCTCT
Lefty2	CACAAGTTGGTCCGTTTCG	GGTACCTCGGGGTCACAAT
Mixl1	CATGTACCCAGACATCCACTTG	ACTCTGGCGCCTGGACTT
Nanog	AAGCAGAAGATGCGGACTGT	ATCTGCTGGAGGCTGAGGTA
Nestin	TCCCTTAGTCTGGAAGTGGCTA	GGTGTCTGCAAGCGAGAGTT
NF-YA	GGCACAATTCTCCAGCAAG	GGCTCCTGTCTGAACGATCT
NF-YB	GCTTCATCACGTCGGAAGCAAGCG	GTCCATCTGTGGCGGAGACTGC
NF-YC	CCCACTGGCTCGTATTAAGAA	GGCTCGAAGAGTCAGCTCAG
Nkx2.2	GCAGCGACAACCCCTACA	ATTTGGAGCTCGAGTCTTGG
Oct4	CCAATCAGCTTGGGCTAGAG	CCTGGGAAAGGTGTCCTGTA
Pax6	GTTCCCTGTCCTGTGGACTC	ACCGCCCTTGGTTAAAGTCT
Prdm14	GGCCATACCAGTGCGTGTA	TGCTGTCTGATGTGTGTTCG
Tbx3	AGATCCGGTTATCCCTGGGAC	CAGCAGCCCCCACTAACTG
Tcl1	ACCTTGGGGGAAGCTATGTC	CTTGGAGCCCAGTGTAGAGG
Actin (control #1)	AAGGCCAACCGTGAAAAGAT	GTGGTACGACCAGAGGCATAC
HAZ (control #2)	CGTTGTAGGAGCCCGTAGGTCAT	TCTGGTTGCGGAAGCATTGGG
TBP (control #3)	CTGAAGAAAGGGAGAATCATGG	TGTCTTTGTTGCTCTTCCAAAA

Supplemental Experimental Procedures

Mouse ES Cell Culture, RNAi, and AP staining

Mouse ESC culture, siRNA transfection, and alkaline phosphatase (AP) staining were performed as previously described (Freudenberg et al., 2012). Briefly, E14Tg2a ESCs were maintained on gelatin-coated plates in the ESGRO complete plus clonal grade medium (Millipore). For siRNA transfections, ESCs were cultured in M15 medium: DMEM (Invitrogen) supplemented with 15%FBS, 10µM 2-mercaptoethanol, 0.1mM nonessential amino acids (Invitrogen), 1x EmbryoMax nucleosides (Millipore), 1U/ml of ESGRO mLIF (Millipore). ESCs (~$25x10^3$) were transfected with siRNAs at 50nM using lipofectamine 2000 (Invitrogen) at day 0, re-plated and re-transfected at 48h, and collected after 96h (see Figure S2A). AP staining was performed using Alkaline Phosphatase Detection Kits from Stemgent (00-0055) according to the manufacturer's instructions. Gene specific siRNAs used: NF-YA (Invitrogen, MSS247473), NF-YB (Qiagen, SI01327193), NF-YC (Qiagen, SI05348217), non-targeting control (Dharmacon, D-001810-02-50).

Chromatin Immunoprecipitation (ChIP)

Mouse ESCs ($1x10^7$) were cross-linked with 1% formaldehyde in DMEM for 10 min, and the reaction was quenched by the addition of glycine at a final concentration of 125 mM for 5 min. Cells were scraped, pelleted, washed twice with PBS, and resuspended in 1ml of lysis buffer A [50mM Hepes pH7.5; 140mM NaCl; 1mM EDTA; 10% Glycerol; 0.5% IGEPAL CA-630; 0.25% Triton X-100; 1x Complete protease inhibitor mixture (Roche), 200nM PMSF]. After 10 min on ice, the cells were pelleted and resuspended in 1ml of lysis buffer B [10mM Tris-HCl pH8.0; 200mM NaCl; 1mM EDTA; 0.5mM EGTA; 1x protease inhibitors, 200nM PMSF]. After 10min at room temperature, cells were sonicated in lysis buffer C [10mM Tris-HCl pH8.0; 100mM NaCl; 1mM EDTA; 0.5mM EGTA; 0.1% sodium deoxycholate; 0.5% N-lauroylsarcosine; 1x protease inhibitors, 200nM PMSF] using Diagenode Bioruptor for 16 cycles (30sec ON; 50sec OFF) to obtain ~200–500 bp fragments. Cell debris were pre-cleared by centrifugation at 14,000 rpm for 20 min, and 25µg of chromatin was incubated with either NF-YA (Santa Cruz, G-2, sc-17753X), NF-YB (Santa Cruz, FL-207X, sc-13045X), NF-YC (Santa Cruz, N-19X, sc-7715X), Oct4 (Santa Cruz, N-19, sc-8628X), Sox2 (Santa Cruz, Y-17, sc-17320X), or histone H3 (Abcam, ab1791) antibodies overnight at 4˚C. Protein A/G-conjugated magnetic beads (Pierce Biotech) were added the next day for 2 hours. Subsequent washing and reverse cross-linking were performed as previously described (Heard et al., 2001). ChIP enrichment for a primer-set was evaluated using quantitative PCR as percentage of input, and normalized to a negative primer-set. See **Table S1** for a list of ChIP primers used.

Quantitative RT-PCR

Total RNAs were prepared from cells using Trizol (Invitrogen), and cDNAs were generated using the iScript kit (Bio-Rad) according to the manufacturer's instructions. Quantitative PCRs were performed on the Bio-rad CFX-96 or CFX-384 Real-Time PCR System using the Bio-rad SsoFast EvaGreen supermix. Three or more biological replicates were performed for each experiment. Data are normalized to *Actin*, *Haz* and *TBP* expression, and plotted as mean +/- S.E.M. See **Table S2** for a list of gene specific primers used.

Western Blot

Cell pellets, lysed in RIPA buffer (25mM Tris-HCl, pH 7.4, 150mM NaCl, 1% NP-40, 1% Sodium deoxycholate) with protease inhibitors, were sonicated using Bioruptor (Diagenode) for three cycles (30 seconds ON; 50 seconds OFF). The lysate was boiled with SDS-PAGE sample buffer, loaded onto NuPAGE gel, and transferred to 0.22µM PVDF membranes. Each membrane was treated with appropriate primary and secondary antibodies. Antibodies used: NF-YA (Santa Cruz, H-209, sc-10779X), NF-YB (Santa Cruz, FL-207X, sc-13045X), NF-YC (Santa Cruz, N-19X, sc-7715X), and Ran (BD Bioscience, 610341). The membrane was then incubated with a horseradish-peroxidase-conjugated secondary antibody and developed with enhanced chemi-luminescence PLUS reagent (Amersham). Loading was normalized based on Ran.

Immunoflourescence

Mouse ESCs transfected with *NF-YA* or control siRNA were grown on gelatin-coated glass cover-slips, and stained for appropriate antibodies for 1hr at 37°C as previously described (Cinghu et al., 2012)(Cinghu et al., 2012), followed by washing in phosphate buffered saline (PBS). Antibodies used: NF-YA (Santa Cruz, G-2X, sc-13057X), NF-YC (Santa Cruz, N-19X, sc-7715X), Nanog (BD Bioscience, 560259). The cover-slips were then treated with appropriate secondary antibody (Alexa 488 or Alexa 594; Invitrogen) for another 1hr at 37°C. Staining of nuclei was accomplished by incubation with DAPI (5mg/ml) for 10min. The slides were then washed extensively in PBS and mounted using Prolong gold anti-fade (Invitrogen). Specimens were viewed using a Zeiss N710 confocal microscope.

Cell Cycle Analysis

Cell cycle analysis was performed using flow cytometry as previously described (Cinghu et al., 2014). Briefly, 48 or 72 hours after siRNA transfection, cells were fixed with 70% ethanol overnight. The next day, cells were washed with PBS, treated with 10µg/ml RNase A (Roche, 10109169001) for 1 hour at room temperature and then stained with 50µg/ml propidium iodide (Sigma, P4170) for at least 10 minutes before loading on a FACSCalibur flow cytometer

(BD Biosciences). Raw data was analyzed using the CellQuest Pro software, and the percentage of each cell cycle phase was calculated with the Flow Jo software.

Co-Immunoprecipitation

ESCs ($1.2x10^7$) were lysed with 1 mL lysis buffer [20 mM Tris-HCl, 2 mM EDTA, 137 mM NaCl, 10% glycerol, 1% Triton-X] for 30 min at 4^oC. Lysates were incubated with antibodies against NF-YA (Santa Cruz, H-209, sc-10779X), NF-YC (Santa Cruz, N-19X, sc-7715X), Oct4 (Santa Cruz, N-19, sc-8628X), or IgG (Santa Cruz, sc-2027) overnight at 4^oC. Magnetic Dynabeads (Life Technologies) were added for 3h at 4^oC. Beads were washed three times with lysis buffer, and proteins were eluted with Laemmli sample buffer at 100^oC for 15 min. Western blots were performed according to standard protocols and were developed using the Odyssey Infrared Imaging System (Li-Cor Biosciences).

DNase I Hypersensitivity

Mouse ESCs treated with non-targeting control siRNA or *NF-YA* siRNA were collected 48 hours post-transfection in cold PBS. Nuclei isolation and DNase I digestion were performed as previously described (Burch and Weintraub, 1983), with minor modifications. Nuclei were isolated by incubation of 10^7 cells for 10 min on ice with 5 ml RSB buffer [10 mM Tris–HCl pH 7.4, 10 mM NaCl, 3 mM $MgCl_2$, 0.15 mM spermine and 0.5 mM spermidine, 1mM PMSF, 0.5% IGEPAL], and pelleted by centrifugation at 300*g* and 4˚C for 10 min. Nuclei were then resuspended in 1 ml DNase reaction buffer [40mM Tris-HCl pH7.4, 10mM NaCl, 6mM $MgCl_2$, 1mM $CaCl_2$, 0.15mM Spermine, 0.5mM Spermidine] and counted. Additional resuspension buffer was used to generate equal concentrations of nuclei between samples. Nuclei from $5x10^5$ cells were aliquoted into microcentrifuge tubes and incubated at 37°C for 5 min with varying amounts of DNase (0U to 75U, Worthington). Digestion was stopped by addition of an equal volume of termination buffer [10 mM Tris pH 7.4, 50 mM NaCl, 100 mM EDTA, 2% SDS, 10 µg/ml RNAse cocktail]. The nuclei were then incubated at 55˚C for 15 min, followed by addition of 2 µl of 20 mg/ml Proteinase K. Reaction mixtures were incubated overnight at 55°C, followed by a phenol–chloroform extraction followed by chloroform extraction of the DNA. The DNA was then precipitated and resuspended in 100 µl H2O.

Microarray Analysis

Raw microarray data files were processed and normalized using RMA and Affymetrix Mouse Genome 430 2.0 Array annotation using applicable R/Bioconductor packages to generate single expression intensity measure per gene per sample. All subsequent analyses were carried out on

the $\log_2$ scale. Differential expression analysis (NF-Y TKD vs. control) was performed using limma R package (Smyth, 2005), followed by Benjamin-Hochberg multiple testing correction to control the false discovery rate (FDR). Genes were considered differentially expressed if they had an FDR≤0.05 and were at least 2.0 fold up- or down-regulated. To compare gene expression changes upon *NF-Y* depletion to those observed after KD or knockout (KO) of other pluripotency-associated factors in previously published studies, respective reference datasets were downloaded from GEO and processed as previously described (Freudenberg et al., 2012). Correlation between global gene expression changes upon KD/KO of various factors were computed and visualized as a heatmap. Published mircoarray datasets used for comparative analysis: Oct4 KD and Nanog KD (Loh et al., 2006); Sox2 KD, Tbx3 KD, Esrrb KD, and Tcl1 KD (Ivanova et al., 2006); Ncl KD (Cinghu et al., 2014); Brg1 KO and LIF withdrawal (Ho et al., 2011); Klf2/4/5 TKD (Jiang et al., 2008); Tet1 KD (Freudenberg et al., 2012); Tcf3 KO (Yi et al., 2011); Suz12 KO (Pasini et al., 2007); Sall4 KD (Lim et al., 2008); embryoid body differentiation (Hailesellasse Sene et al., 2007). Principal component analysis (PCA) of expression profiles from control and NF-Y depleted ESCs and previously published data from wild-type and differentiating ESCs (Aiba et al., 2009; Nishiyama et al., 2009) was performed using R and visualized using R package "rgl."

ChIP-Seq Data Analysis

Single-end 36 bp reads generated from NF-YA, NF-YB, and NF-YC ChIP-Seq were aligned to the mouse reference genome (mm9 assembly) using Bowtie version 0.12.8 (Langmead et al., 2009), and only those reads that mapped to unique genomic locations with at most two mismatches were retained for further analysis. For visualization on the UCSC Genome Browser, and generation of screenshots and read density plots, the data was normalized to reads per million (RPM) and plotted as histograms. For binding site definition (peak calls), aligned reads were processed using SISSRs (Jothi et al., 2008; Narlikar and Jothi, 2012) using default settings. Genome-wide distribution of binding sites was determined with reference to RefSeq gene annotations. Binding sites located withing 500 bp of transcription start sites (TSSs) were defined as promoter-proximal or proximal sites, with the rest defined as distal sites. Genes binding NF-Y within 500 bp of their TSSs were defined as proximal NF-Y target genes, and those that bind NF-Y within 50 Kb but not within 500 bp of their TSSs were defined as distal NF-Y target gene. Binding sites for two transcription factors were defined to be colocalized if the centers of the corresponding peaks are within 500 bp of each other. CpG island annotations were downloaded from UCSC genome (Karolchik et al., 2014). Published ESC ChIP-Seq datasets used for comparative analysis: Oct4, Sox2, Nanog, Tcf3, and Suz12 (Marson et al., 2008); Prdm14 (Ma et al., 2011); Esrrb, Klf4, CTCF, cMyc, nMyc, Zfx, Smad1 (Chen et al., 2008); Stat3 and H3K27me3 (Ho et al., 2011); H3K4me1 and P300 (Creyghton et al., 2010) , H3K4me3 (Agarwal and Jothi,

2012); H3K27ac (ENCODE, GSE31039); DNase (ENCODE, GSE37074); Hi-C (Dixon et al., 2012); Brg1 (Ho et al., 2009); and Ino80 (Wang et al., 2014). Published neuron ChIP-Seq datasets used for comparative analysis: NF-YA and H3K27me3 (Tiwari et al., 2012); CTCF (ENCODE, GSE49847); NPAS4, CREB, SRF, CBP, H3K4me1 and H3K27ac (Kim et al., 2010), DNase (ENCODE, GSE37074).

Functional and pathway enrichment analysis

Gene Ontology (GO) functional enrichment analysis was performed using DAVID (Huang da et al., 2009), and pathway enrichment analysis was performed using PANTHER classification system (Mi et al., 2013).

Motif Analysis

Relevant sequences spanning 200 nucleotides around the centers of NF-Y binding sites were retrieved from the reference genome, and *De-novo* motif search was performed using MEME (Bailey and Elkan, 1994) using zoops (zero or one motif occurrence per sequence) option. Search for known TF motifs, obtained from TRANSFAC (Matys et al., 2006) and JASPAR (Mathelier et al., 2014), was performed using the MAST (Bailey and Gribskov, 1998).

Supplemental References

Agarwal, S.K., and Jothi, R. (2012). Genome-wide characterization of menin-dependent H3K4me3 reveals a specific role for menin in the regulation of genes implicated in MEN1-like tumors. PLoS One *7*, e37952.

Aiba, K., Nedorezov, T., Piao, Y., Nishiyama, A., Matoba, R., Sharova, L.V., Sharov, A.A., Yamanaka, S., Niwa, H., and Ko, M.S. (2009). Defining developmental potency and cell lineage trajectories by expression profiling of differentiating mouse embryonic stem cells. DNA Res *16*, 73-80.

Bailey, T.L., and Elkan, C. (1994). Fitting a mixture model by expectation maximization to discover motifs in biopolymers. Proc Int Conf Intell Syst Mol Biol *2*, 28-36.

Bailey, T.L., and Gribskov, M. (1998). Combining evidence using p-values: application to sequence homology searches. Bioinformatics *14*, 48-54.

Burch, J.B., and Weintraub, H. (1983). Temporal order of chromatin structural changes associated with activation of the major chicken vitellogenin gene. Cell *33*, 65-76.

Chen, X., Xu, H., Yuan, P., Fang, F., Huss, M., Vega, V.B., Wong, E., Orlov, Y.L., Zhang, W., Jiang, J.*, et al.* (2008). Integration of external signaling pathways with the core transcriptional network in embryonic stem cells. Cell *133*, 1106-1117.

Cinghu, S., Goh, Y.M., Oh, B.C., Lee, Y.S., Lee, O.J., Devaraj, H., and Bae, S.C. (2012). Phosphorylation of the gastric tumor suppressor RUNX3 following H. pylori infection results in its localization to the cytoplasm. J Cell Physiol *227*, 1071-1080.

Cinghu, S., Yellaboina, S., Freudenberg, J.M., Ghosh, S., Zheng, X., Oldfield, A.J., Lackford, B.L., Zaykin, D.V., Hu, G., and Jothi, R. (2014). Integrative framework for identification of key cell identity genes uncovers determinants of ES cell identity and homeostasis. Proc Natl Acad Sci U S A.

Creyghton, M.P., Cheng, A.W., Welstead, G.G., Kooistra, T., Carey, B.W., Steine, E.J., Hanna, J., Lodato, M.A., Frampton, G.M., Sharp, P.A.*, et al.* (2010). Histone H3K27ac separates active from poised enhancers and predicts developmental state. Proc Natl Acad Sci U S A *107*, 21931-21936.

Dixon, J.R., Selvaraj, S., Yue, F., Kim, A., Li, Y., Shen, Y., Hu, M., Liu, J.S., and Ren, B. (2012). Topological domains in mammalian genomes identified by analysis of chromatin interactions. Nature *485*, 376-380.

Ernst, J., and Kellis, M. (2012). ChromHMM: automating chromatin-state discovery and characterization. Nat Methods *9*, 215-216.

Freudenberg, J.M., Ghosh, S., Lackford, B.L., Yellaboina, S., Zheng, X., Li, R., Cuddapah, S., Wade, P.A., Hu, G., and Jothi, R. (2012). Acute depletion of Tet1-dependent 5-hydroxymethylcytosine levels impairs LIF/Stat3 signaling and results in loss of embryonic stem cell identity. Nucleic Acids Res *40*, 3364-3377.

Hailesellasse Sene, K., Porter, C.J., Palidwor, G., Perez-Iratxeta, C., Muro, E.M., Campbell, P.A., Rudnicki, M.A., and Andrade-Navarro, M.A. (2007). Gene function in early mouse embryonic stem cell differentiation. BMC Genomics *8*, 85.

Heard, E., Rougeulle, C., Arnaud, D., Avner, P., Allis, C.D., and Spector, D.L. (2001). Methylation of histone H3 at Lys-9 is an early mark on the X chromosome during X inactivation. Cell *107*, 727-738.

Hirayama, T., Tarusawa, E., Yoshimura, Y., Galjart, N., and Yagi, T. (2012). CTCF is required for neural development and stochastic expression of clustered Pcdh genes in neurons. Cell Rep *2*, 345-357.

Ho, L., Jothi, R., Ronan, J.L., Cui, K., Zhao, K., and Crabtree, G.R. (2009). An embryonic stem cell chromatin remodeling complex, esBAF, is an essential component of the core pluripotency transcriptional network. Proc Natl Acad Sci U S A *106*, 5187-5191.

Ho, L., Miller, E.L., Ronan, J.L., Ho, W.Q., Jothi, R., and Crabtree, G.R. (2011). esBAF facilitates pluripotency by conditioning the genome for LIF/STAT3 signalling and by regulating polycomb function. Nat Cell Biol *13*, 903-913.

Huang da, W., Sherman, B.T., and Lempicki, R.A. (2009). Systematic and integrative analysis of large gene lists using DAVID bioinformatics resources. Nat Protoc *4*, 44-57.

Ivanova, N., Dobrin, R., Lu, R., Kotenko, I., Levorse, J., DeCoste, C., Schafer, X., Lun, Y., and Lemischka, I.R. (2006). Dissecting self-renewal in stem cells with RNA interference. Nature *442*, 533-538.

Jiang, J., Chan, Y.S., Loh, Y.H., Cai, J., Tong, G.Q., Lim, C.A., Robson, P., Zhong, S., and Ng, H.H. (2008). A core Klf circuitry regulates self-renewal of embryonic stem cells. Nat Cell Biol *10*, 353-360.

Jothi, R., Cuddapah, S., Barski, A., Cui, K., and Zhao, K. (2008). Genome-wide identification of in vivo protein-DNA binding sites from ChIP-Seq data. Nucleic Acids Res *36*, 5221-5231.

Karolchik, D., Barber, G.P., Casper, J., Clawson, H., Cline, M.S., Diekhans, M., Dreszer, T.R., Fujita, P.A., Guruvadoo, L., Haeussler, M.*, et al.* (2014). The UCSC Genome Browser database: 2014 update. Nucleic Acids Res *42*, D764-770.

Kim, T.K., Hemberg, M., Gray, J.M., Costa, A.M., Bear, D.M., Wu, J., Harmin, D.A., Laptewicz, M., Barbara-Haley, K., Kuersten, S.*, et al.* (2010). Widespread transcription at neuronal activity-regulated enhancers. Nature *465*, 182-187.

Langmead, B., Trapnell, C., Pop, M., and Salzberg, S.L. (2009). Ultrafast and memory-efficient alignment of short DNA sequences to the human genome. Genome Biol *10*, R25.

Lim, C.Y., Tam, W.L., Zhang, J., Ang, H.S., Jia, H., Lipovich, L., Ng, H.H., Wei, C.L., Sung, W.K., Robson, P.*, et al.* (2008). Sall4 regulates distinct transcription circuitries in different blastocyst-derived stem cell lineages. Cell Stem Cell *3*, 543-554.

Loh, Y.H., Wu, Q., Chew, J.L., Vega, V.B., Zhang, W., Chen, X., Bourque, G., George, J., Leong, B., Liu, J.*, et al.* (2006). The Oct4 and Nanog transcription network regulates pluripotency in mouse embryonic stem cells. Nat Genet *38*, 431-440.

Ma, Z., Swigut, T., Valouev, A., Rada-Iglesias, A., and Wysocka, J. (2011). Sequence-specific regulator Prdm14 safeguards mouse ESCs from entering extraembryonic endoderm fates. Nat Struct Mol Biol *18*, 120-127.

Marson, A., Levine, S.S., Cole, M.F., Frampton, G.M., Brambrink, T., Johnstone, S., Guenther, M.G., Johnston, W.K., Wernig, M., Newman, J.*, et al.* (2008). Connecting microRNA genes to the core transcriptional regulatory circuitry of embryonic stem cells. Cell *134*, 521-533.

Mathelier, A., Zhao, X., Zhang, A.W., Parcy, F., Worsley-Hunt, R., Arenillas, D.J., Buchman, S., Chen, C.Y., Chou, A., Ienasescu, H.*, et al.* (2014). JASPAR 2014: an extensively expanded and updated open-access database of transcription factor binding profiles. Nucleic Acids Res *42*, D142-147.

Matys, V., Kel-Margoulis, O.V., Fricke, E., Liebich, I., Land, S., Barre-Dirrie, A., Reuter, I., Chekmenev, D., Krull, M., Hornischer, K.*, et al.* (2006). TRANSFAC and its module TRANSCompel: transcriptional gene regulation in eukaryotes. Nucleic Acids Res *34*, D108-110.

Mi, H., Muruganujan, A., Casagrande, J.T., and Thomas, P.D. (2013). Large-scale gene function analysis with the PANTHER classification system. Nat Protoc *8*, 1551-1566.

Narlikar, L., and Jothi, R. (2012). ChIP-Seq data analysis: identification of protein-DNA binding sites with SISSRs peak-finder. Methods Mol Biol *802*, 305-322.

Nishiyama, A., Xin, L., Sharov, A.A., Thomas, M., Mowrer, G., Meyers, E., Piao, Y., Mehta, S., Yee, S., Nakatake, Y.*, et al.* (2009). Uncovering early response of gene regulatory networks in ESCs by systematic induction of transcription factors. Cell Stem Cell *5*, 420-433.

Pasini, D., Bracken, A.P., Hansen, J.B., Capillo, M., and Helin, K. (2007). The polycomb group protein Suz12 is required for embryonic stem cell differentiation. Mol Cell Biol *27*, 3769-3779.

Smyth, G.K. (2005). Limma: linear models for microarray data. Bioinformatics and Computational Biology Solutions using R and Bioconductor, 397-420.

Tiwari, V.K., Stadler, M.B., Wirbelauer, C., Paro, R., Schubeler, D., and Beisel, C. (2012). A chromatin-modifying function of JNK during stem cell differentiation. Nat Genet *44*, 94-100.

Wang, L., Du, Y., Ward, J.M., Shimbo, T., Lackford, B., Zheng, X., Miao, Y.-l., Zhou, B., Han, L., Fargo, D.C.*, et al.* (2014). INO80 Facilitates Pluripotency Gene Activation in Embryonic Stem Cell Self-Renewal, Reprogramming, and Blastocyst Development. Cell Stem Cell *14*, 575-591.

Yi, F., Pereira, L., Hoffman, J.A., Shy, B.R., Yuen, C.M., Liu, D.R., and Merrill, B.J. (2011). Opposing effects of Tcf3 and Tcf1 control Wnt stimulation of embryonic stem cell self-renewal. Nat Cell Biol *13*, 762-770.